Available online at www.sciencedirect.com

SciVerse ScienceDirect

Journal of the European Ceramic Society 32 (2012) 2537–2543

www.elsevier.com/locate/jeurceramsoc

High-strength ZrB_2-based ceramics prepared by reactive pulsed electric current sintering of ZrB_2–ZrH_2 powders

Songlin Ran [a,*], Shuigen G. Huang [b], Omer Van der Biest [b], Jef Vleugels [b,**]

[a] *Anhui Key Laboratory of Metal Materials and Processing, School of Materials Science and Engineering, Anhui University of Technology, 243002 Ma'anshan, China*

[b] *Department of Metallurgy and Materials Engineering, KU Leuven, B-3001 Heverlee, Belgium*

Received 5 August 2011; received in revised form 17 February 2012; accepted 25 February 2012
Available online 20 March 2012

Abstract

Fully densified ZrB_2-based ceramic composites were produced by reactive pulsed electric current sintering (PECS) of ZrB_2–ZrH_2 powders within a total thermal cycle time of only 35 min. The composition of the final composite was directly influenced by the initial ZrH_2 content in the starting powder batch. With increasing ZrH_2 content, ZrB_2–ZrO_2, ZrB_2–ZrB–ZrO_2 and ZrB_2–ZrB–Zr_3O composites were obtained. The ZrB_2–ZrB–ZrO_2 composite derived from a 9.8 wt% ZrH_2 starting powder exhibited an excellent flexural strength of 1382 MPa combined with a Vickers hardness of 17.1 GPa and a fracture toughness of 5.0 MPa $m^{1/2}$. The high strength was attributed to a fine grain size and the removal of B_2O_3 through reaction with Zr. Higher ZrH_2 content starting powders were densified through solution-reprecipitation resulting in the formation of coarser angular ZrB_2–ZrB composites with a Zr_3O grain boundary phase with a fracture toughness of 5.0 MPa $m^{1/2}$ and an acceptable strength in the 852–939 MPa range.

Keywords: Sintering; Borides; Mechanical properties; Microstructure-final

1. Introduction

Zirconium diboride (ZrB_2) ceramics are considered for potential applications under extreme environments like high temperature and corrosion due to their high melting point, corrosion resistance, electrical and thermal conductivity and mechanical properties.[1,2] For high strength and corrosion resistance, a high and preferably full density is essential.[3] However, the strong covalent bonding makes ZrB_2 very difficult to sinter.[1]

The unavoidable oxide impurities, mainly B_2O_3, present on the ZrB_2 starting powder, are reported to have an adverse effect on the densification of ZrB_2 ceramics due to their evaporation/condensation kinetics and boride grain coarsening effect.[4–6] Although most of the B_2O_3 can be removed by evaporation above 1450 °C under active vacuum conditions, some B_2O_3 might remain entrapped in the densifying powder compact during hot-pressing or pulsed electric current sintering (PECS) since the compact is constrained in a loaded graphite die/punch set-up.[7,8] Adding additives like Si_3N_4 and AlN is claimed to eliminate B_2O_3 by reaction and therefore improve the sinterability of ZrB_2, but the reported strengths are not higher than 600 MPa, partially because of hexagonal BN phase formation.[9,10] With the addition of SiC to form ZrB_2–SiC composites, both the densification and the strength of the materials could be significantly enhanced.[6,11] Hot-pressed ZrB_2–SiC composites with WC–Co contamination for example exhibited near full density and a 4-point strength of 1089 MPa.[11] Besides the grain growth inhibition by the secondary phase, B_2O_3 is removed by reaction with SiC and SiO_2.[6]

Recently, the addition of metal Zr to ZrB_2 during hot-pressing was reported not only to assist the removal of B_2O_3 according to reaction (1) but also to react with ZrB_2 to produce a stable ZrB phase.[12]

$$5Zr + 2B_2O_3(l) = 2ZrB_2 + 3ZrO_2 \quad (1)$$

The purpose of this study is to investigate the fabrication of ZrB_2–ZrB ceramic composites by reactive PECS of ZrB_2 with

* Corresponding author.
** Corresponding author. Tel.: +32 16 321244; fax: +32 16 321992.
E-mail addresses: songlin@ahut.edu.cn (S. Ran), jozef.vleugels@mtm.kuleuven.be (J. Vleugels).

0955-2219/$ – see front matter © 2012 Elsevier Ltd. All rights reserved.
doi:10.1016/j.jeurceramsoc.2012.02.035

Table 1
Batch compositions of the ZrB_2-based ceramics.

Grade	Ceramic (vol%)[a]		Starting powder (wt%)	
	ZrB_2	ZrB	ZrB_2	ZrH_2
ZZ0	100	0	100	0
ZZ10	90	10	95.06	4.94
ZZ20	80	20	90.22	9.78
ZZ30	70	30	85.48	14.52
ZZ40	60	40	80.83	19.17

[a] Calculated based on a theoretical densities of 6.09 g/cm^3 for ZrB_2 and 6.65 g/cm^3 for ZrB.

metal Zr derived from the in situ dehydrogenation of commercial ZrH_2 powders. This paper describes the influence of the ZrH_2 content on the densification, composition, mechanical properties and microstructures of the prepared composites.

2. Experimental procedure

2.1. Processing

Commercially available ZrB_2 (Grade B, H.C. Starck, Germany, 2 μm, 1.0 wt% O) and ZrH_2 (Grade G, Chemetall, Germany, 5.5 μm, 97.6 wt% Zr + Hf, >1.9 wt% H) powders were used as raw materials. For the selection of the starting powder composition, ZrB_2 and ZrB were assumed as the only two phases in the bulk materials, taking into account the following reactions during sintering[12]:

$$ZrH_2 = Zr + H_2(g) \quad (2)$$

$$ZrB_2 + Zr = 2ZrB \quad (3)$$

After batching according to Table 1, the powders were mixed in ethanol for 24 h on a multidirectional mixer (Turbula T2A, WAB, Switzerland) using $\Phi = 5$ mm ZrO_2 milling beads (Grade TZ-3Y, Tosoh, Japan). After mixing, the slurry was dried at 65 °C in a rotating evaporator and subsequently sieved with a 325 μm sieve to minimize powder segregation and agglomeration.

The sieved powder mixture was poured into a graphite die/punch set-up ($\Phi = 40$ mm) lined with graphite paper. Details on the die/punch/powder assembly and temperature measurement/control are provided elsewhere.[13] The synthesis and densification were conducted by PECS (Type HP D25/1, FCT Systeme, Rauenstein, Germany) in a dynamic vacuum. In all experiments, a minimum pressure of 4 MPa was applied to ensure constant contact of the electrodes with the die/punch/sample set-up. The temperature and loading cycle are graphically presented in Fig. 1. The temperature of the sample was automatically raised to 450 °C and was controlled up to 1900 °C at a heating rate of 100 °C/min with pulses of 10 ms on and 3 ms off. During the ramping process, the maximum DC currents and DC voltages for the five samples were 4.08–4.11 kA and 5.40–5.98 V, respectively. The temperature was measured axially through the punch by an optical pyrometer, focused on the bottom of the upper punch about 2 mm from the top surface of the sample. A pressure of 50 MPa was applied within 60 s after a dwell of 5 min at 1900 °C. The ceramic was further heated for another 4 min at 1900 °C under 50 MPa. The pressure was removed after 5 min, while the temperature was rapidly cooled to about 600 °C. The obtained bulk material was about 3.0 mm thick.

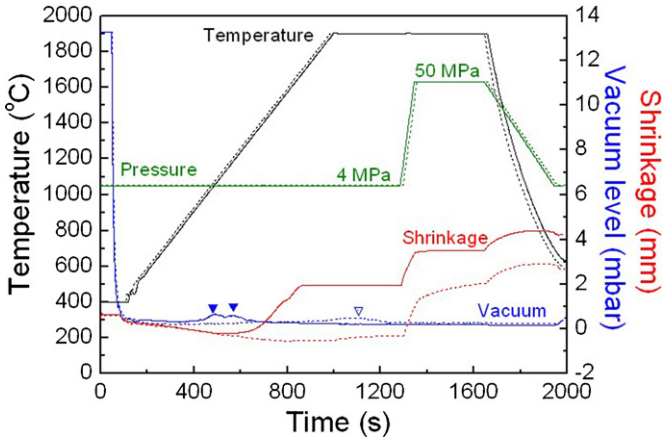

Fig. 1. Comparison of PECS data during densification of ZZ0 (dot) and ZZ40 (solid).

2.2. Characterization

After sandblasting and grinding to remove the surface impurities, the bulk density was measured by the Archimedes method in ethanol. The phase composition was characterized by X-ray diffraction (XRD, 3003 TT, Seifert, Ahrensburg, Germany). The microstructure of the ceramics was examined by scanning electron microscopy (SEM, XL30-FEG, FEI, Eindhoven, The Netherlands) equipped with energy-dispersive X-ray spectroscopy (EDS).

The elastic modulus was measured on a ground disk using the impulse excitation technique (IET, Grindo-Sonic, J.W. Lemmens N.V., Leuven, Belgium). The Vicker's hardness was measured on a hardness tester (Model FV-700, Future-Tech Corp., Tokyo, Japan) with a load of 5 kg and a dwell time of 10 s. The indentation toughness was evaluated from the radial crack pattern accompanying the Vickers indentations and calculated according to the Anstis equation.[14] The reported values are the mean and standard deviations of 10 indentations. The flexural strength was measured on ground rectangular bars (2.5 mm × 1.5 mm × 25 mm) using a 3-point bending set-up (model 4467, Instron, Norwood, MA) with a span of 20 mm and a loading speed of 0.1 mm/min. The reported values are the mean and standard deviations of at least 5 bending bars.

3. Results and discussion

During the PECS process, the changes in temperature, pressure, vacuum level and shrinkage were recorded to allow elucidating the reaction and densification process. Typical PECS cycles for ceramic ZZ0 and ZZ40 are compared in Fig. 1. Due to the fast heating and cooling rate, the total duration of the PECS thermal cycle was less than 35 min.

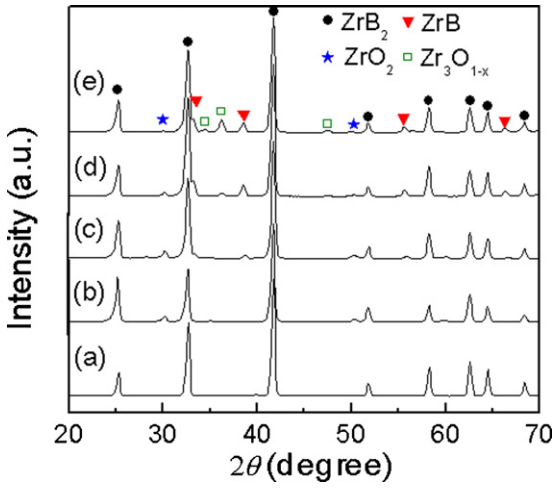

Fig. 2. XRD patterns of ZZ0 (a), ZZ10 (b), ZZ20(c), ZZ30 (d), and ZZ40 (e).

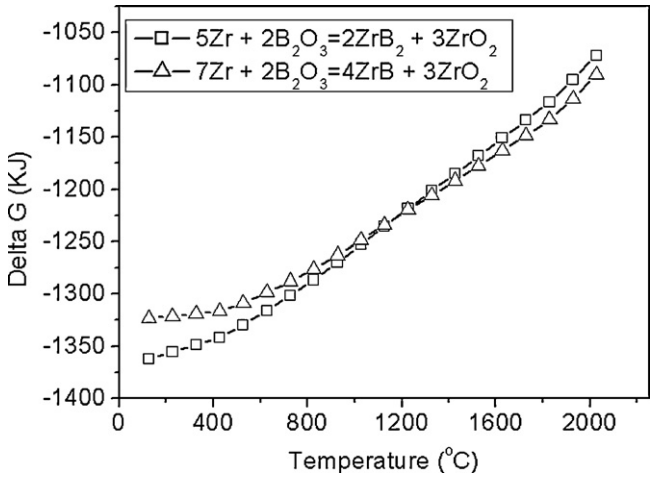

Fig. 3. Gibbs free energy change of reactions (1) and (5).

For both ceramics, the temperature linearly increased at 100 °C/min during the whole ramping process as pre-programmed, implying no self-propagating high-temperature synthesis (SHS) reaction between ZrB_2 and ZrH_2 was ignited in the present experiments. The dehydrogenation of ZrH_2 powder is a two-step process,[7] as confirmed by the two peaks in the vacuum curve for ZZ40, marked by the filled symbols in Fig. 1. During the initial dwell period at 1900 °C, there is a vacuum drop for ZZ0 but not for ZZ40 as indicated by the open symbol in Fig. 1. Since the ZZ0 precursor only comprised commercial ZrB_2 powder, the volatile species should have originated from the B_2O_3 present on the starting powder. For ZZ40 however, the added ZrH_2 and especially the dehydrogenated metal Zr reacted with B_2O_3 according to reaction (1) to form solid ZrO_2 explaining the lack of any volatile species at 1900 °C.

Comparison of the shrinkage curves reveals that the addition of ZrH_2 to ZrB_2 significantly increased the densification behavior. Prior to increasing the mechanical load after 5 min at 1900 °C, there was almost no shrinkage for ZZ0. Upon addition of 19 wt% ZrH_2 however, a clear shrinkage was observed between 1050 and 1700 °C, reaching already a constant level at 1700 °C (see Fig. 1). This plateau level is explained further in the text. After holding an additional 4 min at 1900 °C at 50 MPa, the shrinkage curve kept increasing for ZZ0 while it immediately reached a stable and constant level for ZZ40, as shown in Fig. 1, implying that the ZZ0 ceramic was not yet fully densified and ZZ40 achieved complete densification.

The XRD patterns of all PECS ceramics are compared in Fig. 2, whereas the phase constitution, as obtained by Rietveld analysis of the XRD patterns is provided in Table 2. When 4.94 wt% ZrH_2 powder was added to the starting powder batch, i.e. ceramic ZZ10, about 6 wt% ZrO_2 was formed according to reaction (1), as measured by XRD and confirmed by the microstructure in Fig. 2(b). Comparing the XRD pattern of ZZ0 and ZZ10 indicates that the role of reaction (1) was quite substantial since the ZrH_2 content in ZZ10 is less than 5 wt% and only 0.6 wt% ZrO_2 phase was detected in ZZ0.

Of the investigated ceramics, the ZrO_2 content reached a maximum of 11 wt% in ZZ20, where about 2.4 wt% of an additional ZrB phase was formed. With increasing ZrH_2 contents above 10 wt%, the ZrO_2 phase content decreases, whereas the ZrB content increases up to about 10 wt%. Although the Zr–B binary phase diagram implies that the ZrB phase only exists between 800 and 1250 °C with a peritectoid transformation, stabilization of ZrB at room temperature was proven to be possible either using a special fabrication process or in the presence of carbon, oxygen and nitrogen.[12,15] During the PECS process, the graphite die/punch set-up and starting powders provide a source of carbon and oxygen, stabilizing the ZrB phase in the composite. The ZrB phase content remains almost constant at 9–10 wt% as the ZrH_2 content increased from 14.52 to 19.17 wt%, corresponding to ZZ30 and ZZ40, whereas the content of an additional Zr_3O phase increased from 2.8 to 9.7 wt%.

A possible reason for this could be that the ZrB phase stabilization reached a maximum under the current experimental conditions. After reaching a certain content, the metal Zr did no longer react with ZrB_2 to form ZrB but reacted with ZrO_2 to form oxygen-deficient Zr_3O according to reaction (4) in the ZZ30 and ZZ40 ceramics.

$$ZrO_2 + 5Zr = 2Zr_3O \quad (4)$$

An alternative explanation could be the following reaction:

$$7Zr + 2B_2O_3 = 4ZrB + 3ZrO_2 \quad (5)$$

According to this reaction, of which the Gibbs free energy change is very close to that of reaction (1) as shown in Fig. 3, the formation of ZrB is limited by the amount of Zr introduced in the mixture via ZrH_2 at low ZrH_2 content, whereas the ZrB formation is limited by the initial B_2O_3 amount in the mixture at high ZrH_2 content.

Based on the XRD patterns and the above discussion, it can be concluded that the reaction sequence starts with reaction (1) followed by reactions (3) and (4). When an excess of ZrH_2 was added, i.e. high enough to consume most ZrO_2, the presence of metallic Zr in the ceramics cannot be excluded, and a very small amount of Zr was indeed determined by means of Rietveld analysis of the XRD data (see Table 2). As a result, the final composition of the ceramic composite is directly determined

Table 2
Properties and phase constitution of the ZrB_2-based ceramics.

Grade	ZrH_2 (wt%)	Density (g cm^{-3})	E (GPa)	Hardness (GPa)	Toughness (MPa m$^{1/2}$)	Strength (MPa)	Phase constitution (wt%) (XRD-quantification)
ZZ0	0	4.70	–	–	–	–	99.3 ZrB_2 + 0.6 ZrO_2 + 0.1 Zr
ZZ10	4.94	6.09	512	15.2 ± 0.4	4.3 ± 0.3	894 ± 98	93.4 ZrB_2 + 6.3 ZrO_2 + 0.2 Zr
ZZ20	9.78	6.17	498	17.1 ± 0.3	5.0 ± 0.5	1382 ± 93	86.5 ZrB_2 + 2.4 ZrB + 6.9 t-ZrO_2 + 4 m-ZrO_2 + 0.1 Zr
ZZ30	14.52	6.22	482	16.0 ± 0.7	4.8 ± 0.5	939 ± 59	84.0 ZrB_2 + 10.2 ZrB + 2.8 Zr_3O + 3.0 ZrO_2
ZZ40	19.17	6.25	469	15.1 ± 0.3	4.7 ± 0.2	852 ± 58	80.5 ZrB_2 + 9.1 ZrB + 9.7 Zr_3O + 0.5 ZrO_2 + 0.2 Zr

by the ZrH_2 or metal Zr content in the densifying compact. These data are consistent with the traces of ZrO_2 and absence of Zr_3O reported for a ZrB_2–ZrB composite, hot pressed from a ZrB_2–8.32 wt% Zr starting powder.[12]

Representative backscattered electron micrographs of polished cross-sections and secondary electron micrographs of fracture surfaces of the composites are shown in Fig. 4. Relatively large residual pores are located at the triple junctions and along some grain boundaries and smaller pores are trapped inside the ZrB_2 grains in the ZZ10 ceramic, shown in Fig. 4(a). The ZrO_2 phase can be clearly distinguished as the substantially smaller grain sized phase at the ZrB_2 grain boundaries and triple junctions, as confirmed by EDS point analysis. It should be pointed out that some color contrast is observed in the backscattered SEM images (Fig. 4(a), (c), (e) and (g)) for the ZrB_2 phase, which is induced by a different orientation of the ZrB_2 crystals and not by a difference in phase composition. During PECS, metal Zr reacted with B_2O_3 present on the ZrB_2 starting powder to produce ZrB_2 and ZrO_2. The freshly formed ZrB_2 particles were consumed by the ZrB_2 grain growth, whereas the ZrO_2 grains remain at the grain boundaries of the ZrB_2 grains.

The microstructure of the ZZ20 ceramic reveals an additional ZrB brighter atomic number contrast phase, as shown in Fig. 4(c). Some pores entrapped inside ZrB_2 grains can still be observed.

In ZZ30 and ZZ40, shown in Fig. 4(e) and (f), and additional white atomic number contrast phase is formed. This phase was identified as Zr_3O, which tends to surround the ZrB grains. The ZrB_2 matrix grains became more angular compared to the ZZ10 and ZZ20 grades, as framed by the rectangles in Fig. 4(g). Similar angular ZrB_2 grains were reported for ZrB_2/ZrC/Zr composites prepared by liquid infiltration, in contrast to platelet shaped ZrB_2 grains that were formed in ZrB_2/ZrC/Zr composites prepared by the direct reaction method.[16] The formation of angular rectangular shapes was attributed to Ostwald ripening induced by the presence of a liquid phase.[16] In the present work, the melting point of Zr (1855 °C) and the eutectic point (1680 °C) between ZrB_2 and metal Zr are lower than the sintering temperature of 1900 °C, confirming the presence of a liquid phase promoting solution-reprecipitation. During the cooling process, the remaining liquid finally solidified into ZrB at 1250 °C and Zr_3O at 970 °C, according to the Zr–B and Zr–O phase diagrams respectively.[15,17] The oxygen source for the formation of the ZrO_2 and Zr_3O phase originates from the ZrB_2 as well as the ZrH_2 starting powder. Although no oxygen analysis was performed on the ZrH_2 powder, it is known to readily oxidize in an oxygen atmosphere. The presence of a liquid phase also enhanced densification of the composites. No residual porosity could be observed on polished cross-sections.

The average boride grain size decreases with increasing ZrH_2 content in the starting powder from 4.9 (ZZ10) to 9.8 (ZZ20) wt%, due to the additional grain boundary pinning effect of the ZrB phase in ZZ20. Further increasing the ZrH_2 content (ZZ30 and ZZ40) results in the formation of a liquid phase and concomitant solution-reprecipitation coarsening, resulting in more angular and a larger ZrB_2 and ZrB grain morphology.

In the Zr–B binary phase diagram, there is an eutectic point between ZrB_2 and metal Zr at 1680 °C.[15] This is clearly reflected by the small step in the PECS shrinkage curve for ZZ40, shown in Fig. 1. The plateau in the shrinkage curve reached around 1700 °C actually reflects full densification. The additional apparent densification upon increasing the load from 4 to 50 MPa should be fully attributed to a deformation of the whole SPS set-up during loading.

The measured density of the PECS ceramics is summarized in Table 2. The ZZ0 monolithic ZrB_2 ceramic reached a density of 4.70 g cm^{-3}, which is only 77% of the theoretical density. This is substantially lower than the relative density of >97% reported for single-phase ZrB_2 PECS at 1900 °C.[18] This difference can however be attributed to the different location of temperature measurement. In the present work, the temperature was measured by an optical pyrometer focused at the bottom of a borehole in the upper punch about 2 mm from the top surface of the disc,[13] whereas the temperature was measured in a hole drilled in the die in Ref. 18.

Since the temperature measuring method used in this study proved to be quite accurate with a temperature difference between the center of a 5 mm thick sample and the controlling pyrometer of less than 5 °C at temperatures ≤1500 °C and the core temperature of a conductive sample during PECS was much higher than the temperature of the die surface as well as sample edge,[13] the actual temperature applied to the ZrB_2 compact in Ref. 18 must have been substantially higher than the reported 1900 °C explaining the higher density. This assumption was recently confirmed by a reported relative density of 70% for a monolithic ZrB_2 ceramic obtained from the same starting powder as in this study, PECS at 1900 °C.[19]

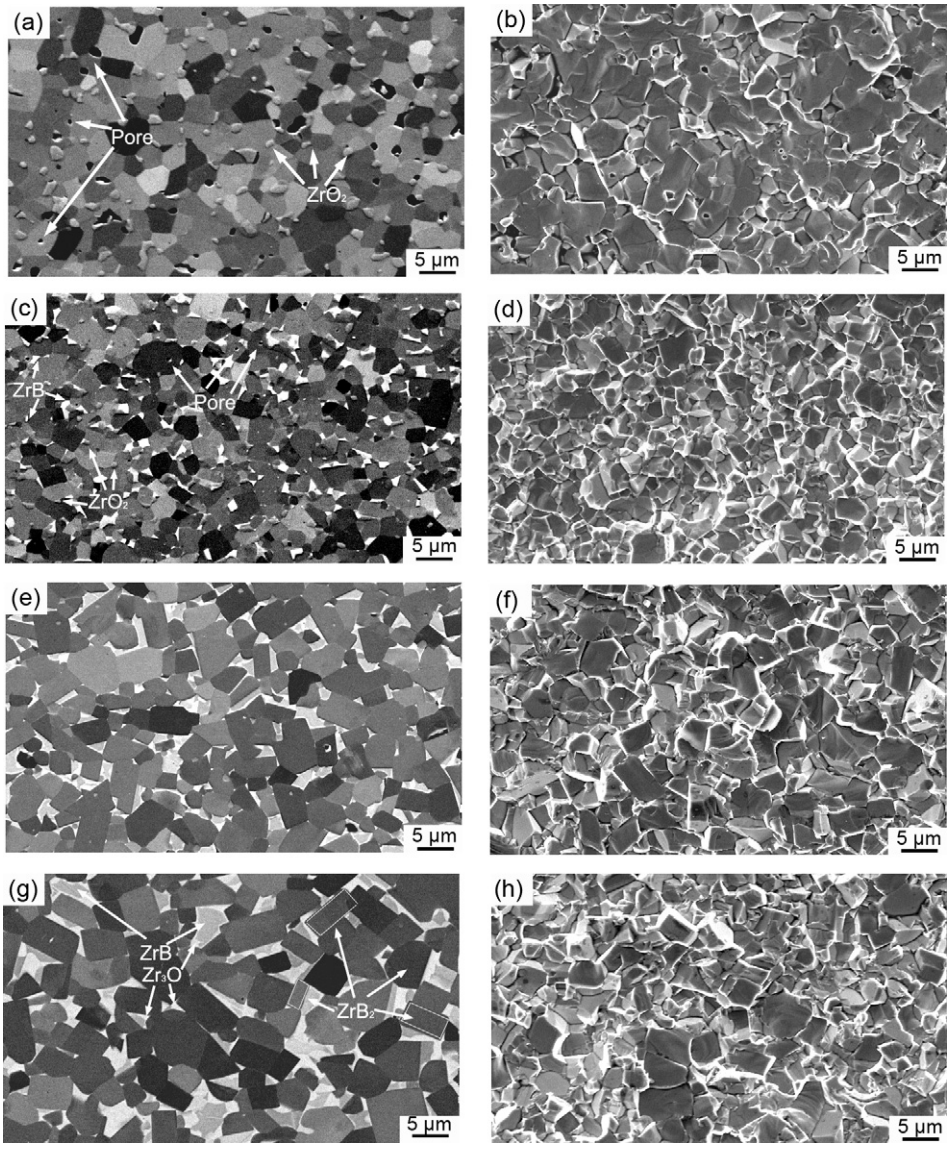

Fig. 4. Polished cross sections (a, c, e, g) and fracture surfaces (b, d, f, h) of ZZ10 (a, b), ZZ20 (c, d), ZZ30 (e, f) and ZZ40 (g, h).

The density of ZZ10 was 6.09 g cm^{-3}, which can be considered to be near fully dense because of its two-phase composition (see Fig. 2(b)) and the comparable density of ZrB_2 (6.09 g cm^{-3}) and ZrO_2 (6.10 g cm^{-3}). Although the presence of the unexpected Zr_3O phase in the higher ZrH_2 starting powder content grades ZZ30 and ZZ40 makes it impossible to calculate their relative densities, the PECS shrinkage curves and SEM images (see Fig. 4) confirm that these ceramics are fully dense.

The Young's modulus of the composites decreased with increasing ZrH_2 content in the starting powder, most probably because of the lower intrinsic stiffness of ZrO_2, ZrB and ZrO_3 compared to ZrB_2.

The Vicker's hardness of the fully dense ZZ20, ZZ30 and ZZ40 composites decreases with increasing ZrH_2 content in the starting powder due to the formation of a liquid phase during densification and the concomitant boride grain growth. Although the ZZ10 ceramic contains some residual porosity, the hardness is comparable to that of ZZ40. The obtained hardness is lower than that of ZrB_2–SiC composites prepared by the same reactive PECS process, due to the incorporation of harder SiC in the latter composites.[7] The hardness however is slightly higher than for hot-pressed ZrB_2 ceramics with Zr, B_4C or Zr and B_4C additives.[12]

With increasing ZrH_2 content in the starting powder batch, the fracture mode of the densified composite changed, as illustrated in Fig. 4(b), (d), (f) and (h). The sample ZZ10 exhibits a rather smooth fracture surface, as shown in Fig. 4(b), corresponding to a transgranular fracture mode which is also reflected in a lower fracture toughness of 4.3 MPa m$^{1/2}$. The fracture surfaces of the ZZ20, ZZ30 and ZZ40 ceramics are much rougher presenting a mixed trans- and intergranular mode resulting in an acceptable constant fracture toughness of 5.0 MPa m$^{1/2}$. The measured fracture toughness, ranging from 4.3 to 5.0 MPa m$^{1/2}$, is higher than that of ZrB_2–SiC composites measured using the same method.[7,20]

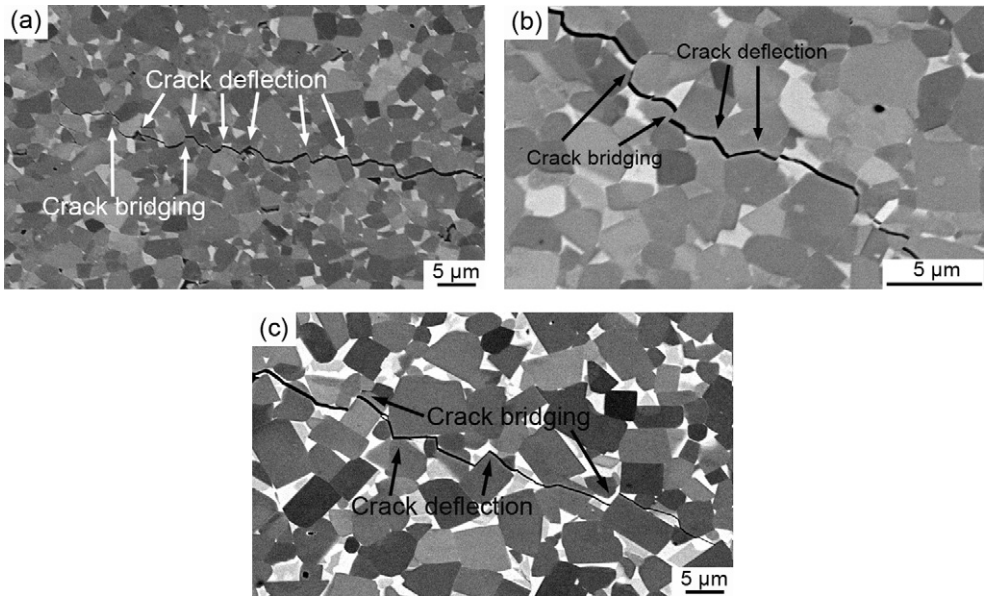

Fig. 5. Polished cross-sections of ZZ20 (a, b) and ZZ40 (c) with indentation crack path.

The indentation crack path in the ZZ20 and ZZ40 ceramic is shown in Fig. 5. The main observed toughening mechanisms are crack deflection and crack bridging, as indicated by the arrows. Residual stresses in the composites induced by the mismatch of the thermal expansion coefficients (CTE) between ZrB_2 and ZrO_2, Zr_3O or ZrB could promote these two mechanisms. In addition, the removal of B_2O_3 according to reaction (1) to form crystalline ZrB_2 and ZrO_2 could decrease the interface strength, enhancing the fracture toughness by increased intergranular crack propagation.[21]

An excellent average 3-point bending strength of 1382 MPa was measured for the 9.78 wt% ZrH_2 powder based ZZ20 composite. The higher and lower ZrH_2 content grades had a lower but still quite appreciable strength of 852–939 MPa. The ZZ20 ceramic had the highest strength due to the full densification, highest toughness and especially finest microstructure. As a comparison, the highest reported strengths for ZrB_2-based composites was 1009 MPa (3-point bending, ZrB_2–SiC) and 1089 MPa (4-point bending, ZrB_2–SiC), respectively.[11,22]

The high strength of the PECS ZrB_2–ZrH_2 based composites is attributed to the complete removal of B_2O_3 in the composites. Generally, the oxygen impurities, mainly ZrO_2 and B_2O_3, are blamed to promote ZrB_2 coarsening which retards densification and deteriorates strength.[23] Due to the fact that B_2O_3 has a low melting point of 450 °C and a high vapour pressure, researchers believed that B_2O_3 could be removed by vaporization below the sintering temperature and paid more attention to removing ZrO_2 by chemical reactions. However, although B_2O_3 begins to volatilize above 1200 °C in vacuum, around 10% liquid B_2O_3 may still be retained in the powder compact up to at least 1400 °C.[23] Therefore, it is not unreasonable to assume that a small amount of B_2O_3 remains entrapped in the closed interstitial spaces of the solid particle compact, especially during hot pressing (HP) or PECS in which the powder compact is constrained in a graphite die/punch set-up.[3] For PECS for example, the starting temperature for B_2O_3 volatilization could be delayed to 1750 °C, as indicated by the vacuum curve of ZZ0 in Fig. 1, because the powder compact was tightly sealed off from the furnace atmosphere by the minimum pressure applied to keep tight contact of the electrodes with the die/punch/sample set-up. Since B_2O_3 was still evaporating at the sintering temperature, it is reasonable to believe that some B_2O_3 remained in the bulk ceramic composite. Similar phenomena have been observed in the fabricating process of ZrB_2–SiC and TiB_2–B_4C composites using PECS.[7,8] When adding ZrH_2, all B_2O_3 could be consumed by reaction (1) and the grain boundaries are strengthened. Previous research also proved that densification and strength of ZrB_2 ceramics could be improved when considering B_2O_3 removal.[12,23] In addition, the by-product of reaction (1), i.e. ZrO_2, was recently claimed to be beneficial for strengthening ZrB_2 ceramics.[24]

Similar composites prepared by hot pressing of ZrB_2–Zr powder mixtures were reported to have a substantially lower 3-point strength of 584 MPa.[12] Although the 9.8 wt% ZrH_2 in the present study is comparable with the 8.3 wt% Zr used in the literature study,[12] the following facts may contribute to the higher strength obtained when using ZrH_2 instead of Zr. Firstly, the brittle ZrH_2 is easier to mill than ductile metal Zr, resulting in a more homogeneous starting powder mixture batch. Secondly, ZrH_2 powder is available in smaller sizes than Zr, and can even be further milled down in particle size. Moreover, PECS with a lower sintering temperature and a short thermal cycle allows limiting grain growth more effectively during densification than HP and results in a finer microstructure. The measured average ZrB_2 grain size of the PECS ZZ20 was 3.2 ± 0.7 μm, as illustrated in Fig. 4(c), which is only half of the grain size of the HP grade reported in the literature.[12]

The high-temperature mechanical performance of ZrB_2-based composites is crucial for a successful application in high-temperature environments. Because of the presence of

the unstable ZrB phase in a similar ZrB_2-based composite, their high-temperature properties were questioned.[12] However, another investigation revealed that the moderate softening of a metallic phase at intermediate temperatures was beneficial for the strength.[3] The strength of a ZrB_2–4 wt% Ni composite for example could be enhanced from 371 MPa at room temperature to 624 MPa at 800 °C.[3] According to the Zr–B binary phase diagram, the ZrB phase could be stabilized between 800 and 1250 °C.[15] Therefore, the effect of the metastable phase on the high-temperature properties of the prepared ceramics would be small below 1250 °C. Moreover, the results in Fig. 2 and previous studies confirmed the possibility of stabilizing ZrB at room temperature in the presences of carbon and oxygen, so it is not unreasonable to image that the stable temperature region of the ZrB phase in the as-prepared composites is even higher than 1250 °C. The high-temperature mechanical properties of the prepared composites and the effect of the ZrB phase will be investigated in the future.

4. Conclusions

ZrB_2-based composites were prepared by pulsed electric current sintering of commercial ZrB_2 and ZrH_2 powder mixtures within a total thermal cycle time of only 35 min. Depending on the overall ZrH_2 content in the starting powder, up to 4 reactions were observed. ZrH_2 initially decomposed into metal Zr, which reacted with the B_2O_3 present on the ZrB_2 starting powder to form ZrB_2 and ZrO_2. Providing there is enough Zr, it reacted with ZrB_2 to form a metastable ZrB phase that is stabilized in the presence of carbon and oxygen. Finally, the excess Zr reacted with ZrO_2 to form Zr_3O. As a result, the composition of the PECS composite is directly related to the initial ZrH_2 content. The addition of ZrH_2 proved to be efficient in converting the B_2O_3 oxide layer on the ZrB_2 starting powder into ZrO_2 and ZrB_2, eliminating B_2O_3 evaporation.

The addition of ZrH_2 to ZrB_2 greatly improved the sinterability of ZrB_2 powders. The PECS shrinkage curves and microstructural analysis indicated that more than 4.94 wt% ZrH_2 enhanced the relative density from 77% for the monolithic ZrB_2 to >99% for the ZrB_2–ZrO_2 composites. The ZrB_2–ZrB–ZrO_2 composites prepared from a 9.8 wt% ZrH_2 powder batch had the finest microstructure and the best mechanical properties with a 3-point flexural strength of 1382 MPa, a Vickers hardness of 17.1 GPa and a fracture toughness of 5.0 MPa $m^{1/2}$. Solution-reprecipitation in the higher ZrH_2 content ceramics resulted in fully dense coarser angular ZrB_2–ZrB microstructures with a Zr_3O grain boundary phase with an acceptable strength of 852–939 MPa and a toughness of 5.0 MPa $m^{1/2}$. The active toughening mechanisms were identified as crack deflection and crack bridging.

Acknowledgments

This work was supported by the Research Fund of KU Leuven under project GOA/08/007, the Flanders-China bilateral project BIL 07/06 and the Fund for Scientific Research Flanders (FWO) under project No. G.0305.07.

References

1. Fahrenholtz WG, Hilmas GE, Talmy IG, Zaykoski JA. Refractory diborides of zirconium and hafnium. *J Am Ceram Soc* 2007;**90**:1347–64.
2. Guo S-Q. Densification of ZrB_2-based composites and their mechanical and physical properties: a review. *J Eur Ceram Soc* 2009;**29**:995–1011.
3. Monteverde F, Bellosi A, Guicciardi S. Processing and properties of zirconium diboride-based composites. *J Eur Ceram Soc* 2002;**22**:279–88.
4. Zhang SC, Hilmas GE, Fahrenholtz WG. Pressureless densification of zirconium diboride with boron carbide additions. *J Am Ceram Soc* 2006;**89**:1544–50.
5. Bellosi A, Monteverde F. Ultra-refractory ceramics: the use of sintering aids to obtain microstructure control and properties improvement. *Key Eng Mater* 2004;**264**(268):787–92.
6. Monteverde F. Beneficial effects of an ultra-fine α-SiC incorporation on the sinterability and mechanical properties of ZrB_2. *Appl Phys A* 2006;**82**:329–37.
7. Ran S, Van der Biest O, Vleugels J. ZrB_2–SiC composites prepared by reactive pulsed electric current sintering. *J Eur Ceram Soc* 2010;**30**:2633–42.
8. Huang SG, Vanmeensel K, Malek OJA, Van der Biest O, Vleugels J. Microstructure and mechanical properties of pulsed electric current sintered B_4C–TiB_2 composites. *Mater Sci Eng A* 2011;**528**:1302–9.
9. Monteverde F. Beneficial effects of AlN as sintering aid on microstructure and mechanical properties of hot-pressed ZrB_2. *Adv Eng Mater* 2003;**5**:508–12.
10. Monteverde F, Bellosi A. Effect of the addition of silicon nitride on sintering behaviour and microstructure of zirconium diboride. *Scripta Mater* 2002;**46**:223–8.
11. Chamberlain AL, Fahrenholtz WG, Hilmas GE, Ellerby DT. High-strength zirconium diboride-based ceramics. *J Am Ceram Soc* 2004;**87**:1170–2.
12. Wang XG, Guo WM, Kan YM, Zhang GJ. Hot-pressed ZrB_2 ceramics with composite additives of Zr and B_4C. *Adv Eng Mater* 2010;**12**:893–8.
13. Vanmeensel K, Laptev A, Hennicke J, Vleugels J, Van der Biest O. Modelling of the temperature distribution during field assisted sintering. *Acta Mater* 2005;**53**:4379–88.
14. Anstis GR, Chantikul P, Lawn BR, Marshall DB. A critical evaluation of indentation techniques for measuring fracture toughness: I, direct crack measurements. *J Am Ceram Soc* 1981;**64**:533–8.
15. Champion Y, Hagège S. A study of composite interfaces in the Zr–ZrB_2 system. *J Mater Sci Lett* 1992;**11**:290–3.
16. Kuk Woo S, Hee Kim C, Son Kang E. Fabrication and microstructural evaluation of ZrB_2/ZrC/Zr composites by liquid infiltration. *J Mater Sci* 1994;**29**:5309–15.
17. Zr–O phase diagram. http://www.springermaterials.com/docs/VSP/datasheet/lpf-c/00901000/LPFC_901820.html.
18. Guo S-Q, Nishimura T, Kagawa Y, Yang J-M. Spark plasma sintering of zirconium diborides. *J Am Ceram Soc* 2008;**91**:2848–55.
19. Thompson M, Fahrenholtz WG, Hilmas G. Effect of starting particle size and oxygen content on densification of ZrB_2. *J Am Ceram Soc* 2011;**94**:429–35.
20. Chamberlain AL, Fahrenholtz WG, Hilmas GE. Low-temperature densification of zirconium diboride ceramics by reactive hot pressing. *J Am Ceram Soc* 2006;**89**:3638–45.
21. Guo W-M, Vleugels J, Zhang G-J, Wang P-L, Van der Biest O. Effects of Re_2O_3 (Re = La, Nd, Y and Yb) addition in hot-pressed ZrB_2–SiC ceramics. *J Eur Ceram Soc* 2009;**29**:3063–8.
22. Liu Q, Han W, Han J. Influence of SiCnp content on the microstructure and mechanical properties of ZrB_2–SiC nanocomposite. *Scripta Mater* 2010;**63**:581–4.
23. Zhu S, Fahrenholtz WG, Hilmas GE, Zhang SC. Pressureless sintering of zirconium diboride using boron carbide and carbon additions. *J Am Ceram Soc* 2007;**90**:3660–3.
24. Li W, Zhang X, Hong C, Han W, Han J. Preparation, microstructure and mechanical properties of ZrB_2–ZrO_2 ceramics. *J Eur Ceram Soc* 2009;**29**:779–86.